Supplementary Information (SI) for Chemical Science.

Synergistic catalysis between In single atoms and In nanoparticles for highly selective electrocatalytic CO_2 reduction to formate with high current densities

Yuxin Chen,[a] Junyoung Choi,[b] Fangkui Liang,[c] Xinyi Tan,*[d] Yudi Chen,[e] Jiahui Yang,[a] Song Hong,[a] Xin Zhang,[c] Alex W. Robertson,[f] Yousung Jung*[b] and Zhenyu Sun*[a]

[a] *State Key Laboratory of Organic–Inorganic Composites, Beijing University of Chemical Technology, Beijing 100029, P. R. China. E-mail: sunzy@mail.buct.edu.cn*

[b] *Department of Chemical and Biological Engineering, Institute of Chemical Processes, and Institute of Engineering Research, Seoul National University, 1 Kwanak-ro, Seoul 08826, South Korea*

[c] *College of Mathematics and Physics, Beijing University of Chemical Technology, Beijing 100029, P. R. China*

[d] *School of Materials Science and Engineering, Beijing Institute of Technology, Beijing Key Laboratory of Environmental Science and Engineering, Beijing 100081, P. R. China*

[e] *Beijing Academy of Science and Technology, Beijing 100089, P. R. China*

[f] *Department of Physics, University of Warwick, Coventry CV4 7AL, UK*

Materials. Potassium bicarbonate ($KHCO_3$, > 99.7%), potassium hydroxide (KOH, 85%), indium chloride ($InCl_3$ > 99%), acetone (C_3H_6O > 99.9%), carbon powder, and sodium citrate ($Na_3C_6H_5O_7 \cdot 2H_2O$ 98%) were obtained from Innochem. Hydrochloric acid (HCl, 37%), glycerol ($C_3H_8O_3$ > 99.9%), Ni foam, and sodium borohydride ($NaBH_4$, 98%) were provided by Sinopharm Chemical Reagent Co., Ltd, China. Polytetrafluoroethylene (PTFE)-hydrophobized carbon paper (CP, Toray, YLS-30T GDL) and Nafion D-521 dispersion (5% w/w in water and 1-propanol, ≥ 0.92 meg/g exchange capacity) were purchased from Alfa Aesar China Co., Ltd. Ar (99.999%) and CO_2 (99.999%) were bought from Beijing Haipu Gas Co., Ltd. All chemicals were analytical grade and used without further purification.

Preparation of In−NSC/NPs, In−NSC/NPs-0.1, In−NSC/NPs-0.3, and In−NSC catalysts. 10 g of commercially purchased broad bean shells (BBS) were added into 250 mL of anhydrous ethanol, which was subjected to magnetic stirring at room temperature for 24 h, and then dried for 12 h in an oven at 60 °C. Then, 2 g of the pretreated BBS was transferred to a tube furnace and heated at 800 °C for 2 h under N_2 with a ramp rate of 3 °C min^{-1}. Subsequently, the resulting sample was cleaned with HCl (1 M) to remove any inorganic salts and then with ultrapure water to approach a neutral condition. 200 mg of the resultant sample was then ultrasonicated for 4 h in 15 mL of ultrapure water, yielding a uniform dispersion labeled as NSC. 0.2 mmol of $InCl_3$ and 0.4 mmol of sodium citrate were added into 15 mL of 0.1 M HCl solution and stirred for 30 min at room temperature to ensure a complete dissolution. Then the NSC suspension was added into this solution under magnetic stirring at 40 °C for 6 h. Subsequently, 1 mL of freshly prepared $NaBH_4$ solution (76 mg) was added dropwise into the above mixture under magnetic stirring in an ice bath for 2 h. The generated precipitate was separated by filtration and washed three times with ultrapure water and anhydrous ethanol, respectively. The obtained product was then dried in a vacuum oven at 60 °C overnight and labeled as In−NSC/NPs.

The preparation process of In−NSC/NPs-0.1 and In−NSC/NPs-0.3 is similar to that of In−NSC/NPs, except that the amount of some raw materials added were changed. In the In−NSC/NPs-0.1, The addition amount of $InCl_3$ and sodium citrate were reduced to 0.1 and 0.2 mmol, the concentration of HCl was 0.05 M and the amount of $NaBH_4$ was reduced to 38 mg. In the In−NSC/NPs-0.3, The addition amount of $InCl_3$ and sodium citrate were increased to 0.3 and 0.6 mmol, the concentration of HCl was 0.6 M and the amount of $NaBH_4$ was increased to 114 mg.

0.2 g of In−NSC/NPs catalyst was added into 100 mL, 1 M of H_2SO_4 under magnetic stirring at 80 °C for 12 h, and then the product obtained was washed repeatedly with water and ethanol until neutral and dried overnight at 60 °C in a vacuum oven to obtain the In−NSC single atom catalyst.

Preparation of $NiCo_2O_4$. $NiCo_2O_4$ nanoarrays were synthesized according to the method reported by Wu et al.[1] 240 mg of $Co(NO_3)_3 \cdot 6H_2O$ was dissolved in a solution containing 15 mL of H_2O and 15 mL of ethanol under magnetic stirring for 10 min. Then, the mixture was transferred into a 50 mL of Teflon-lined autoclave. A piece of pre-cleaned Ni foam (2×4 cm^2) was immersed in the solution under bath ultrasonication for 10 min. Following this, 120 mg of urea was dissolved into the above solution. The autoclave was then sealed and heated at 100 °C for 24 h. Subsequently, the Ni foam sample with $NiCo_2O_4$ precursor was taken out of the autoclave and repeatedly cleaned with water and ethanol, which was then annealed at 300 °C for 3 h with a ramp rate of 5 °C min^{-1} under air atmosphere to obtain $NiCo_2O_4$ sample.

Characterization. Powder X-ray diffraction (XRD) patterns were obtained using a D/MAX-RC diffractometer operated at 30 kV and 100 mA with Cu Kα radiation (λ = 0.15418 nm) at a scanning rate of 5° min^{-1}. X-ray photoelectron spectroscopy (XPS) experiments were conducted using a Thermo Scientific ESCALAB 250Xi instrument. The instrument was equipped with an electron flood and a scanning ion gun. The binding energy was corrected for surface charging by referencing the C 1*s* peak of contaminant carbon at 284.8 eV. Scanning electron microscopy (SEM) was performed using an S-4800 microscope with a 3 kV accelerating voltage. Transmission electron microscopy (TEM) and aberration-corrected high-angle annular dark-field scanning TEM (HAADF-STEM) were conducted on a JEOL ARM200 microscope with a 200 kV accelerating voltage. STEM samples were prepared by depositing a droplet of suspension onto an Au grid coated with a lacey carbon film.The elemental contents of the catalysts were detected using inductively coupled plasma optical emission spectroscopy (ICP-OES, Vista-MPX). CO_2 adsorption isotherms were measured on an NOVA 4000e Surface Area & Pore Size analyzer at 25 ºC. Before measurements, the sample was degassed at 200 °C for 12 h.

In situ attenuated total reflection-surface enhanced infrared absorption spectroscopy (ATR-SEIRAS) measurements. In situ ATR-SEIRAS experiments were performed on an INVENIO-S FT-IR SB-840 spectrometer equipped with a MCT detector cooled with liquid nitrogen and a custom-made ATR sampling accessory. Si crystals coated with catalyst, Ag/AgCl electrode, and Pt plate were used as working electrode, reference electrode, and counter electrode, respectively. In situ ATR-SEIRAS spectra were collected during linear sweeping from 0 to −0.8 V (vs. RHE) with a scan rate of 5 mV s^{-1} in a CO_2-saturated 0.1 M $KHCO_3$ solution. Each spectrum was collected with 44 scans (collection duration of 10 s) at a resolution of 8 cm^{-1}, which was presented using the spectrum at OCP as the background.

Electrocatalysis experiments. The electrochemical performance of the ECR was evaluated in flow cell and MEA, respectively. The electrochemical data were recorded on a CHI-760E electrochemical workstation equipped with a high current amplifier CHI680c for all electrochemical tests. For the flow cell system, an electrocatalyst ink was prepared using a mixture of 1 mL of acetone, 20 μL of Nafion D521 solution, 10 mg of catalyst. The ink was then sprayed onto the gas-diffusion layer (GDL, YLS-30T) to yield a catalyst loading of 1 mg cm^{-2}. An Hg/HgO electrode was used as the reference electrode and a Pt sheet (~2 cm^2) was used as the counter electrode. A CO_2 gas flow (40 mL min^{-1}) was fed to the cathode side, and a KOH aqueous solution (1.0 M) was employed as the electrolyte and circulated around both the cathode and anode sides, and an anion exchange membrane (Fumasep FAB-3PK-130) was used to separate the anodic and cathodic chambers. The pH value of the catholyte was kept at 14.0 irrespective of the absence or the presence of CO_2 gas flow fed to the cathode side through the gas-diffusion electrode (GDE). All the electrode potentials were transformed into RHE potentials by using the following formulas: $E(\text{RHE}) = E(\text{Hg/HgO}) + 0.098 + 0.059 \times \text{pH} + 0.85 \times iR$. The 85% iR compensation was conducted in a flow cell experiment at each potential.

The chronopotentiometry method was used for evaluating long-term activity stability of electrocatalysts in 1 M KOH electrolyte. In order to address the issue of salt precipitation of GDE, the ECR was interrupted after 11 h of continuous operation and the GDE was taken out and washed with deionized water to remove the precipitated salts then dried under a heat lamp. 300 μl of diluted PTFE emulsion (Polytetrafluoroethylene (PTFE) diluent was prepared with 5 μl of 60% PTFE dispersion and 300 μl of deionized water) was sprayed on the back of GDE and also dried under a heat lamp to restore the hydrophobicity of GDE then put it into further stability testing.

The membrane electrode assembly (MEA) system consisted of a graphite anode (cathode) bipolar plate with serpentine flow field, the GDE is similar to that used in the flow cell (2×2 cm^2) as the cathode and Ni foam (2×2 cm^2) as the anode. A pre-treated Sustainion X37–50 Grade RT membrane (4×4 cm^2) was used as an anion-exchange membrane. 1 M KOH aqueous solution was used as the anolyte and circulated using a pump at a rate of 20 $mL\cdot min^{-1}$. When test performances, a humidified CO_2 gas flow (40 $mL\cdot min^{-1}$) was fed to the cathode side and an aqueous solution of 1 M KOH was circulated around the anode side.

The ECR//GOR in the MEA system was tested with the GDE is similar to that used in the flow cell (2×2 cm^2) as the cathode and $NiCo_2O_4$ (2×2 cm^2) as the anode. 1 M KOH and 0.2 M glycerol were used as the anolyte and circulated using a pump at a rate of 20 $mL\cdot min^{-1}$. Other test conditions were the same as ECR//OER in the MEA system.

Product analysis and quantification. The gaseous products were analyzed by a gas chromatograph (Agilent 7890B). The faradaic efficiency of gas products (H_2 and CO) was calculated as follows:

$$FE\ gas(\%) = \frac{Q\ gas}{Q\ total} = \frac{v \times t \times \delta / V \times N \times F}{i\ total \times t} \times 100\%$$

where v is the flow rate of CO_2, δ is the measured gas product concentration in the GC sample loop, V is the gas molar volume (24 L mol^{-1}), N is the number of electrons transferred from CO_2 to products, F is the Faraday's constant (96500 C mol^{-1}), and $i\ total$ is the total recorded current.

Liquid products were analyzed by ^1H NMR (AVANCE NEO 400 MHz). Typically, 300 μL of the electrolyte was mixed with 300 μL of D_2O, and DMSO was used as the interval standard. The concentration of formate was elucidated by its NMR peak area relative to the internal standard, and the corresponding faradaic efficiency can be calculated as below:

$$FE\ liquid(\%) = \frac{Q\ liquid}{Q\ total} = \frac{\eta\ DMSO \times S\ liquid/S\ DMSO \times N \times F}{Q\ total} \times 100\%$$

where $\eta\ DMSO$ is the internal standard DMSO mole, $S\ liquid$ is the formate peak area in NMR spectra, $S\ DMSO$ is the DMSO peak area in NMR spectra, N is the number of electrons transferred from CO_2 to products, F is the Faraday's constant (96500 C mol^{-1}), and $Q\ total$ is the total number of electric charge.

The single pass carbon efficiency (SPCE) can be calculated as follows:

$$SPCE = \frac{(J \times 60\ s)/(N \times F)}{(v \times 10\ min)/(24.05\ L/mol)} \times 100\%$$

where J is partial current of formate, N is the number of electrons transferred from CO_2 to format, F is the Faraday's constant (96500 C mol^{-1}), and v is the flow rate of CO_2.

The energy conversion efficiency (ECE) can be calculated as follows:

$$ECE = \frac{1.23 - E\ formate}{E} \times FE\ formate \times 100\%$$

where $E\ formate$ is the standard potential for formate production (−0.2 V vs. RHE), and E is the applied cell voltage in MEA.

The formation rate of formate (R_{formate}) can be calculated as follows:

$$R\ formate = \frac{Q\ total \times 1000}{F \times N \times t \times S} \times FE\ formate$$

where $Q\ total$ is the total charges consumed, F is the Faraday's constant (96500 C mol^{-1}), N is the number of electrons transferred from CO_2 to formate, t is the reaction time, and S is the geometric area of the GDE.

Density functional theory (DFT) calculations. Spin-polarized DFT calculations were conducted using the Vienna ab initio simulation package

(VASP).[2] We employed the generalized gradient approximation with the Perdew-Burke-Ernzerhof (PBE) functional.[3] The projector augmented wave (PAW) method was utilized with a plane-wave energy cutoff of 400 eV.[4] Weak van der Waals interactions were accounted for using Grimme's D3 method with zero-damping.[5] For modeling In−NSC/NPs, we used a $6 \times 3\sqrt{3}$ rectangular supercells of nitrogen and sulfur-doped monolayer graphene with a 20 Å vacuum layer to eliminate interactions between periodic images. The Gamma point was used to integrate the Brillouin zone. We set convergence criteria of 10^{-5} eV for electronic self-consistent calculations and 0.05 eV/Å for structural relaxations. The free energy of reaction intermediates was calculated according to:

$$G = E_{\mathrm{DFT}} + E_{\mathrm{ZPE}} - TS$$

where E_{DFT} represents the total energy from DFT calculations, E_{ZPE} is the zero-point energy, T is temperature (298.15 K), and S is entropy. Vaspkit 1.3.3 was used to determine E_{ZPE} values.[6]

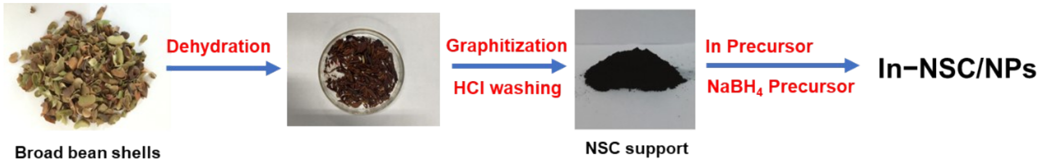

Figure S1. Schematic of the synthesis process for the In−NSC/NPs catalysts.

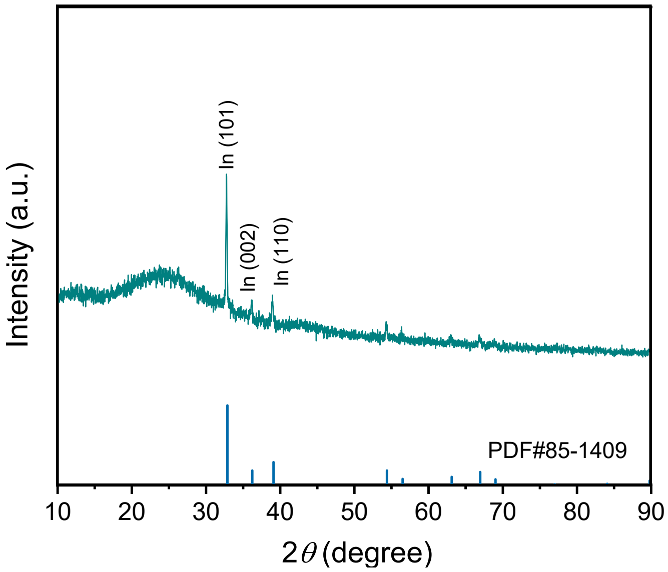

Figure S2. XRD pattern of the as-synthesized In−NSC/NPs.

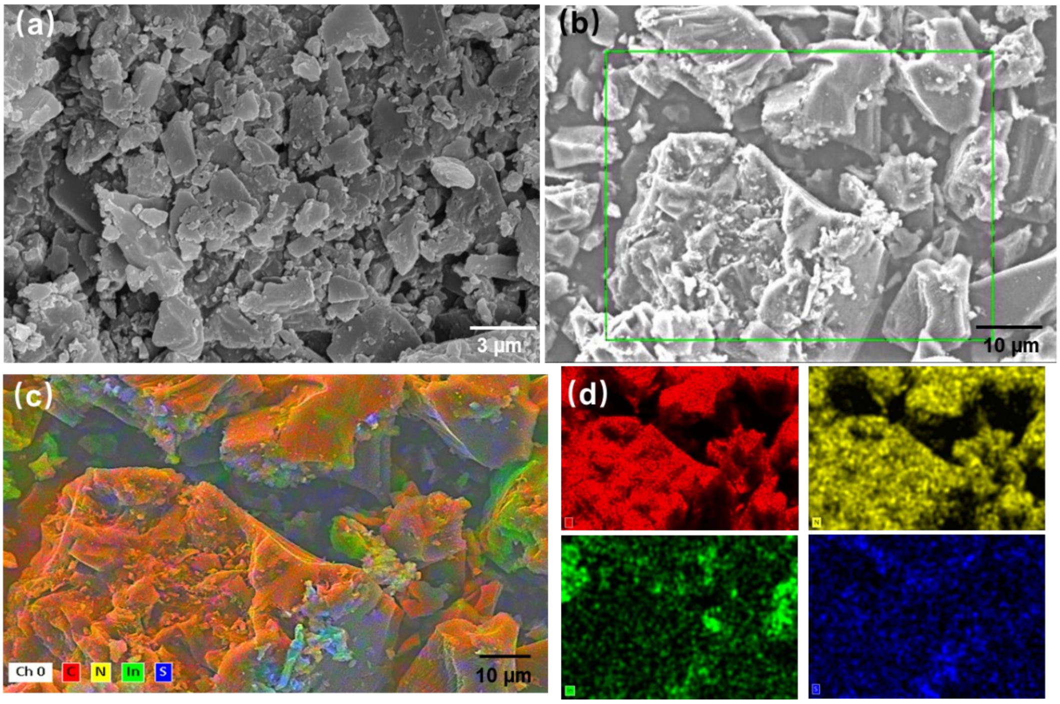

Figure S3. (a, b) is the SEM images of In−NSC/NPs. (c) SEM image with overlapped elemental maps of C, N, In, and S of the region encased in the green box in (b). (d) EDS mapping images of (c).

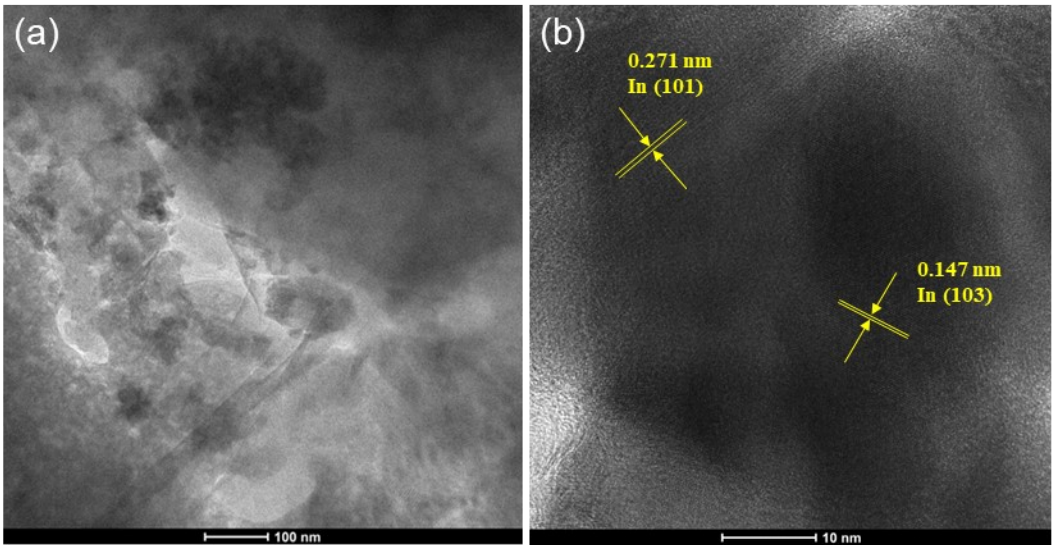

Figure S4. (a) TEM and (b) HRTEM images of In−NSC/NPs.

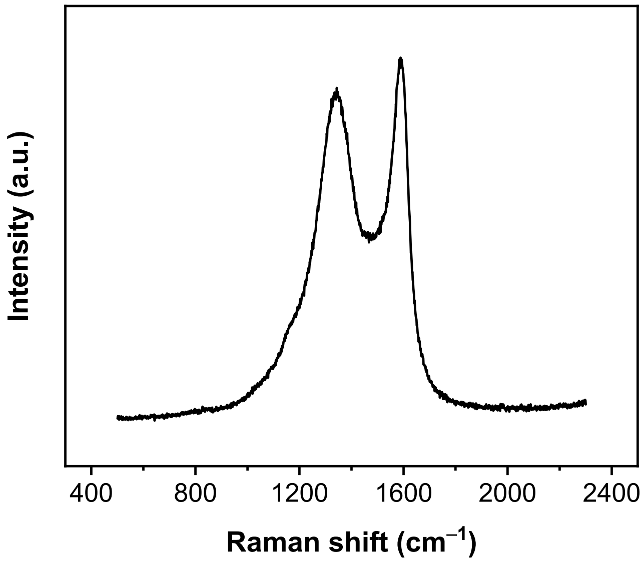

Figure S5. Raman spectrum of In−NSC/NPs.

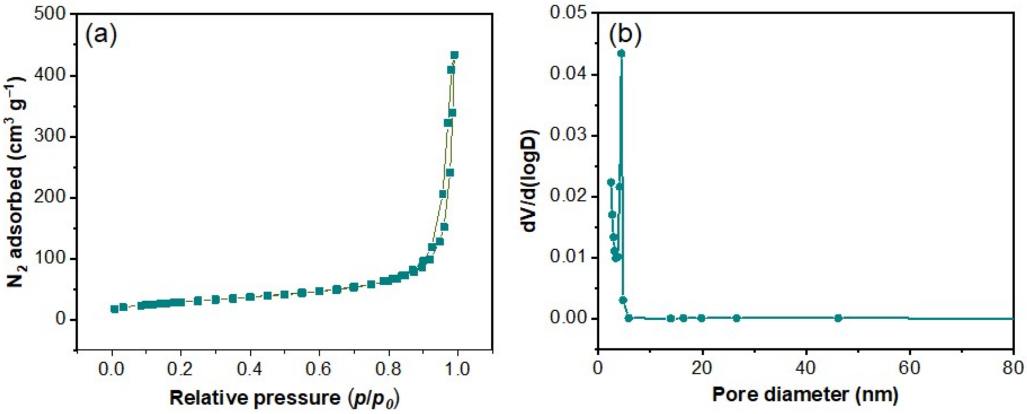

Figure S6. (a) N_2 adsorption−desorption isotherms and (b) pore size distribution of In−NSC/NPs.

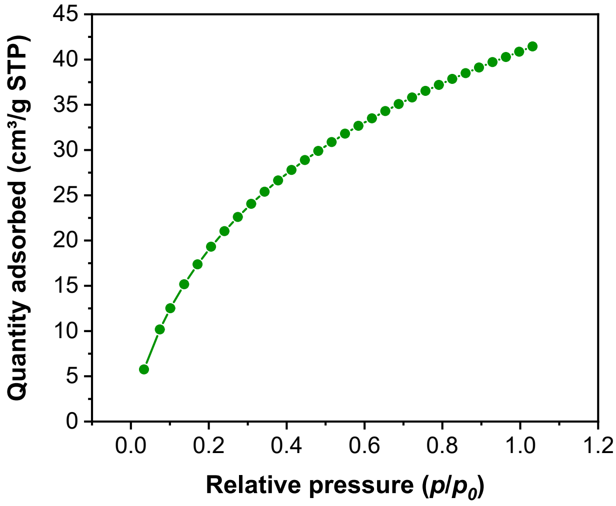

Figure S7. CO_2 adsorption isotherm of In−NSC/NPs.

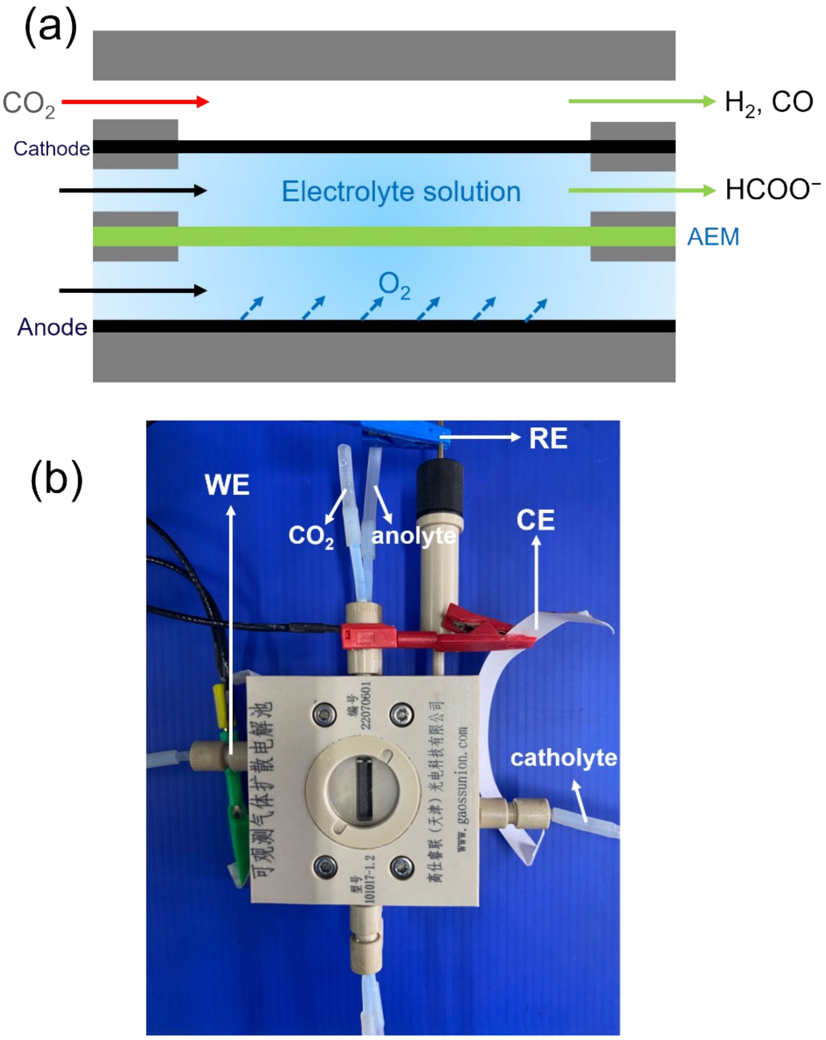

Figure S8. (a) Schematic diagram and (b) photo of a flow cell reactor.

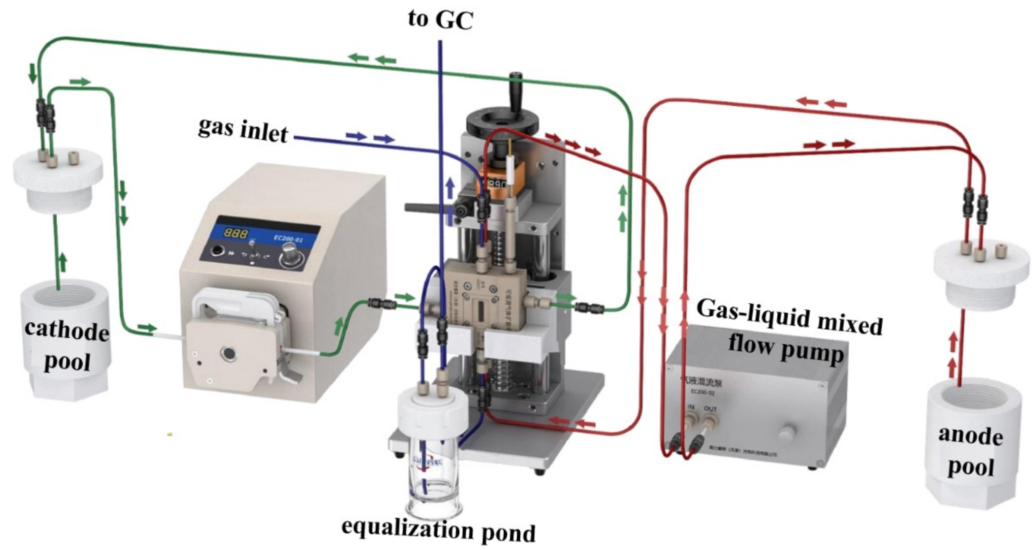

Figure S9. Schematic diagram of an ECR flow cell electrolytic system.

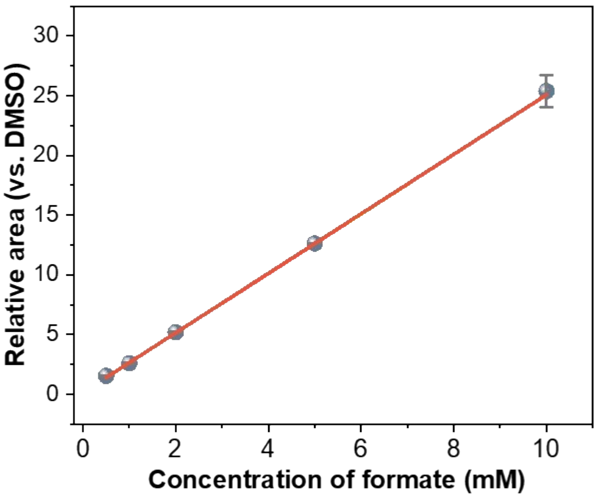

Figure S10. The calibration curve for formate with DMSO as an internal standard.

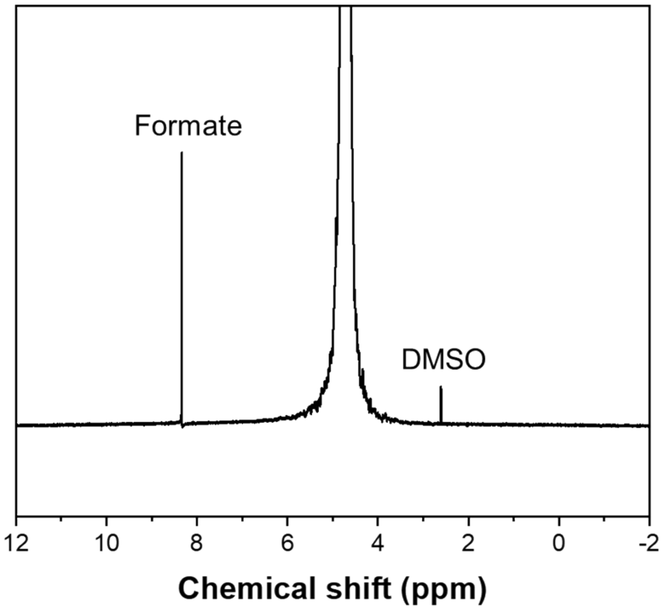

Figure S11. ^1H NMR spectrum of the liquid products after CO_2 electrolysis on In−NSC/NPs.

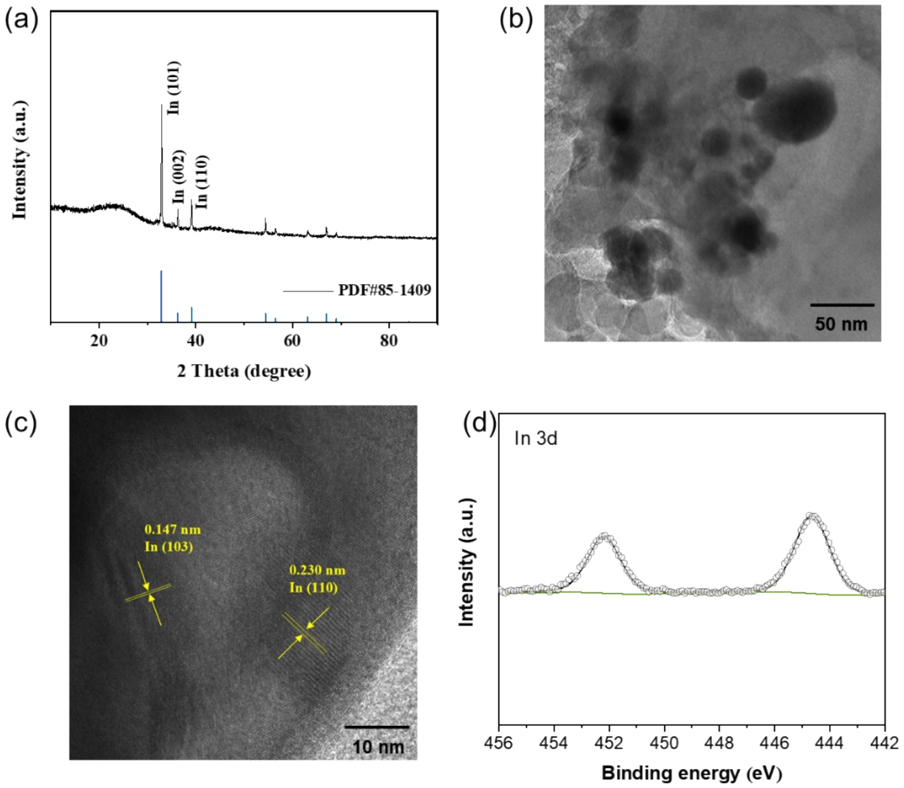

Figure S12. (a) XRD pattern, (b) TEM, (c) HRTEM images, and (d) In 3d XPS spectrum of In−NSC/NPs after CO_2 electrolysis.

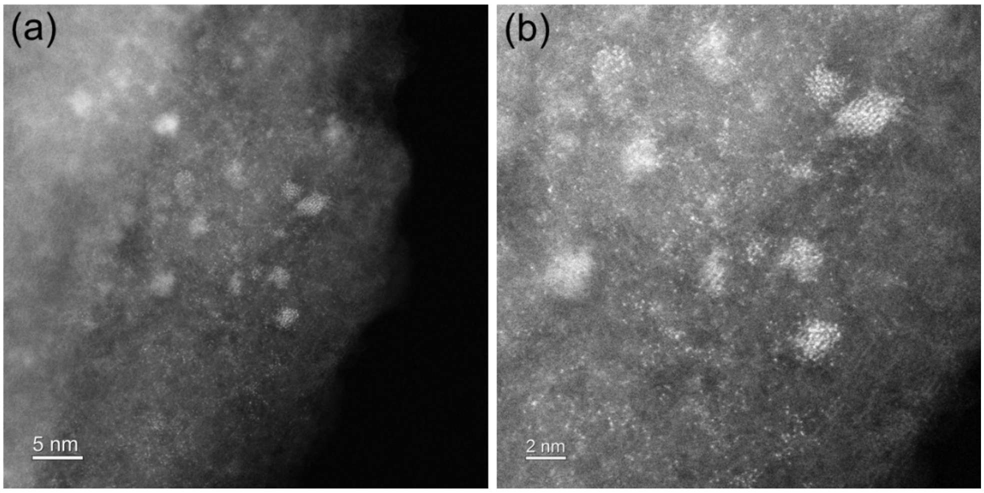

Figure S13. (a) Low-magnification and (b) high-magnification STEM images of In−NSC/NPs after CO_2 electrolysis. It can be clearly recognized that abundant atomic In sites are still well dispersed on the surface of N and S co-doped carbon sheets even after CO_2 electrolysis.

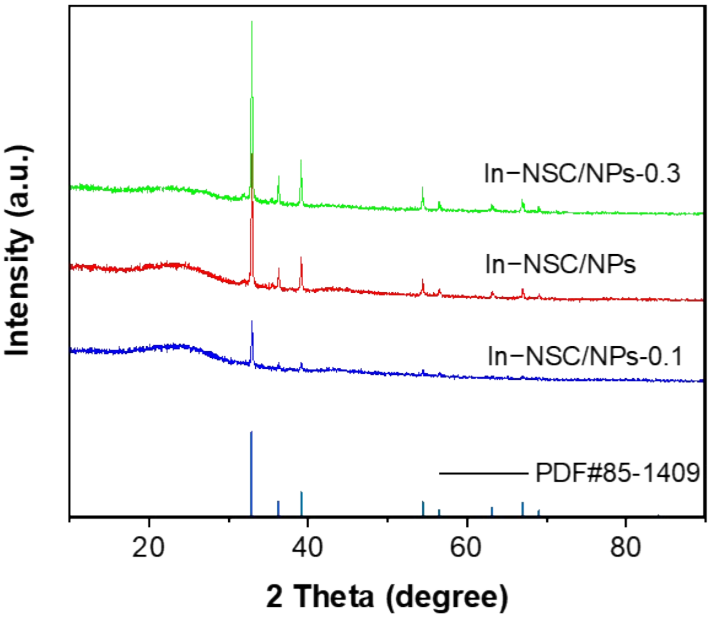

Figure S14. XRD patterns of In−NSC/NPs-0.1, In−NSC/NPs, and In−NSC/NPs-0.3.

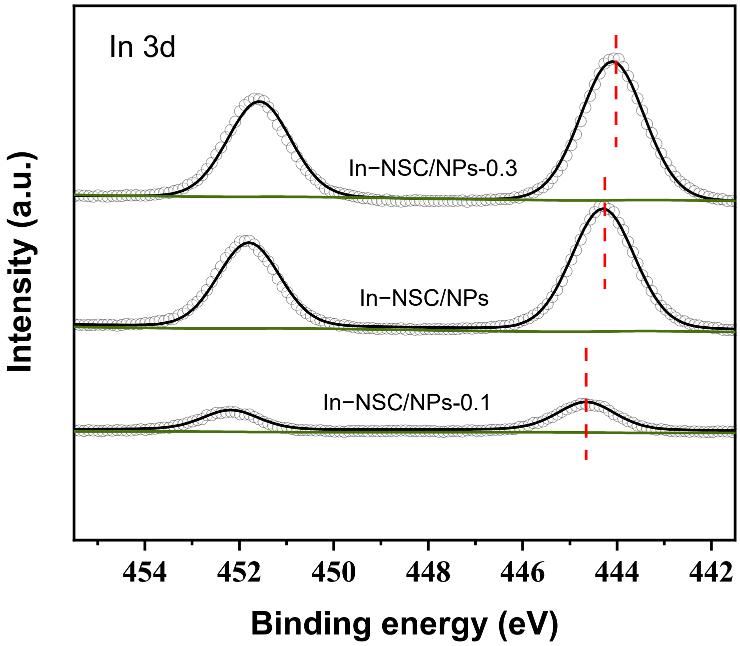

Figure S15. In 3d XPS spectra of In−NSC/NPs-0.1, In−NSC/NPs, and In−NSC/NPs-0.3.

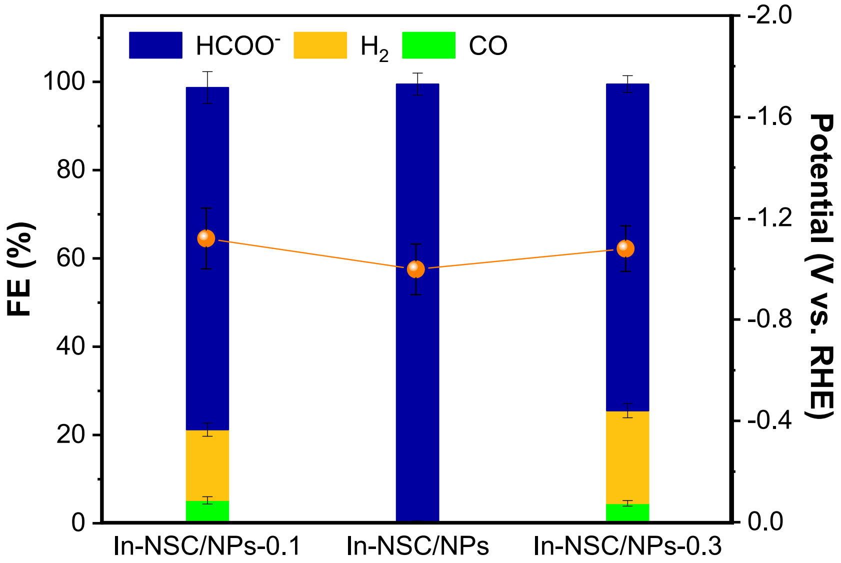

Figure S16. Constant current electrolysis tests of In−NSC/NPs-0.1, In−NSC/NPs, and In−NSC/NPs-0.3 in a CO_2 atmosphere under 0.6 A·cm^{-2}. The data are represented as mean ± standard deviation of three independent measurements.

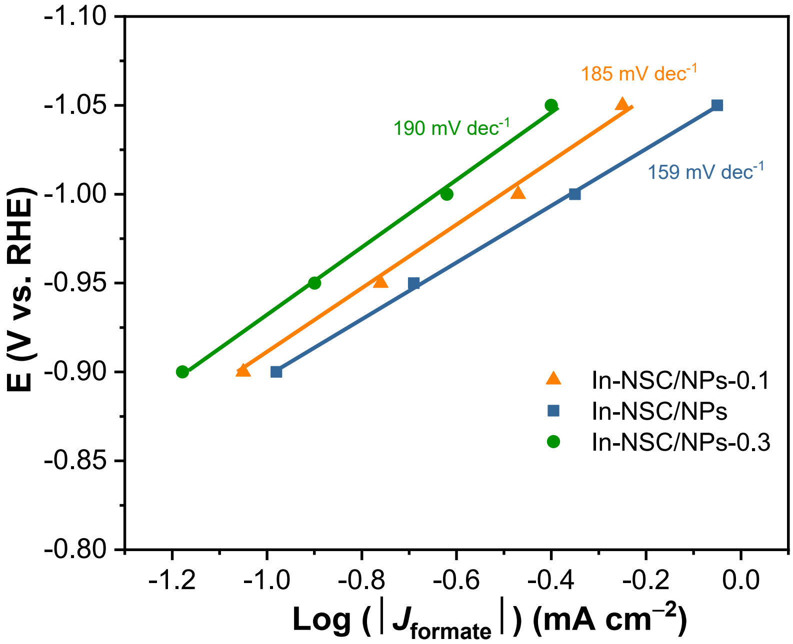

Figure S17. Tafel plots of In−NSC/NPs-0.1, In−NSC/NPs, and In−NSC/NPs-0.3.

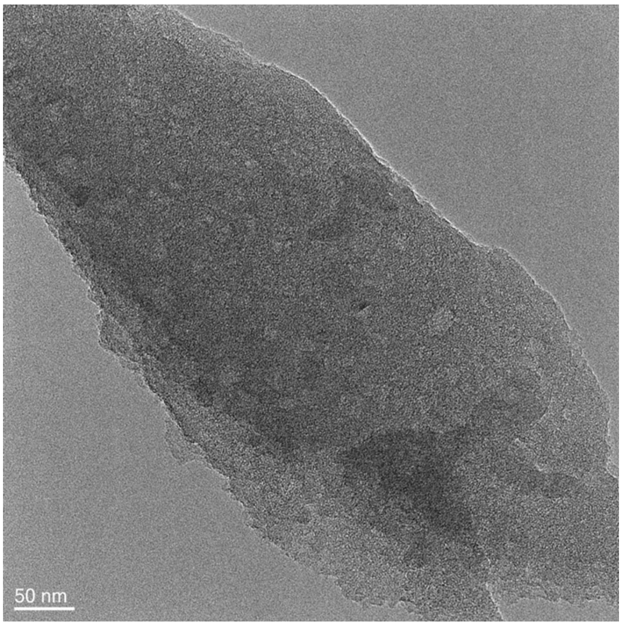

Figure S18. HRTEM image of In−NSC.

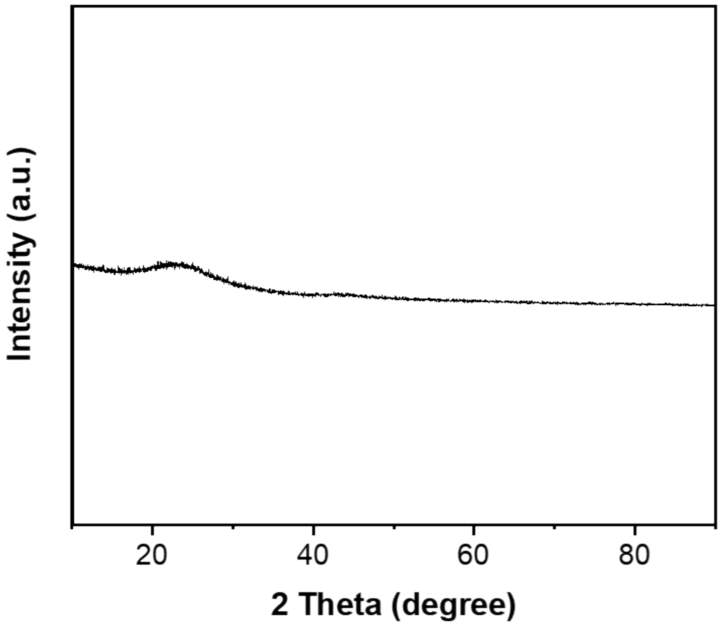

Figure S19. XRD pattern of In−NSC.

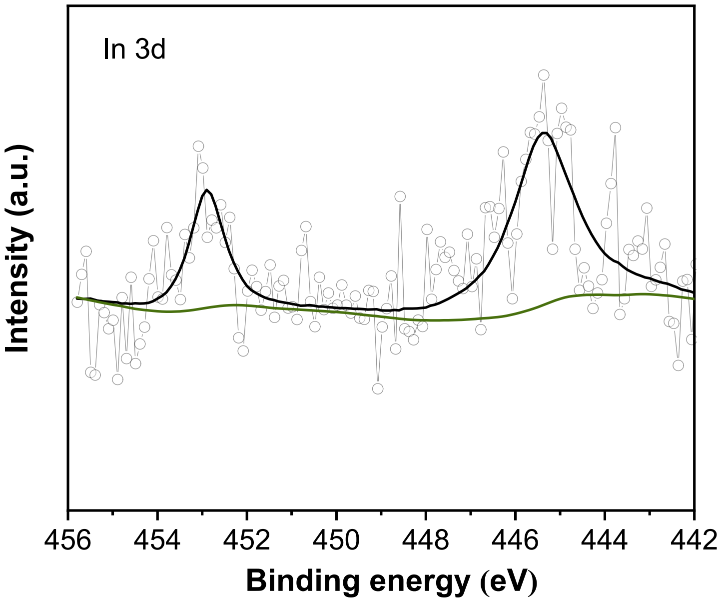

Figure S20. In 3d XPS spectrum of In−NSC.

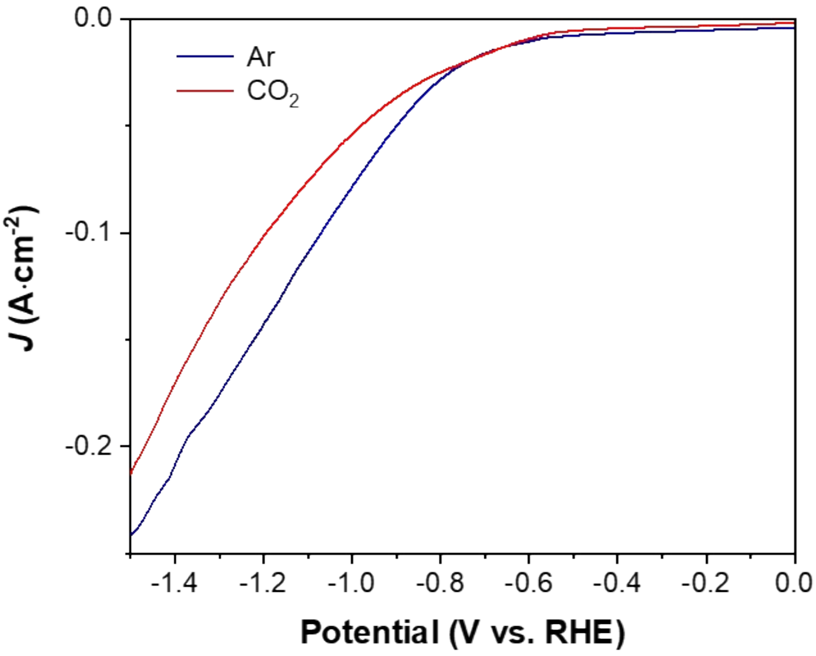

Figure S21. LSV curves of In−NSC under CO_2 and Ar atmosphere at a scan rate of 20 mV·s^{-1}.

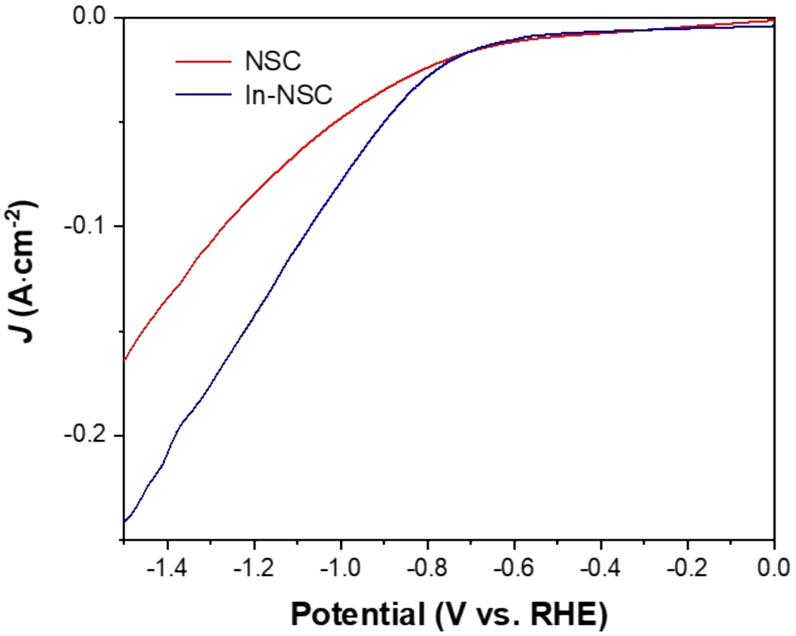

Figure S22. LSV curves of NSC carrier and In−NSC under Ar atmosphere at a scan rate of 20 mV·s^{-1}.

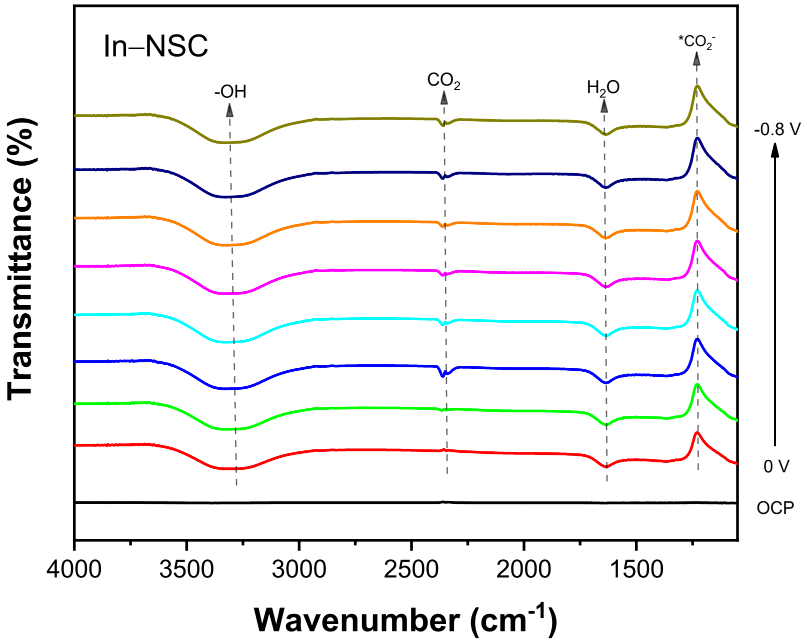

Figure S23. ATR-SEIRAS measurement results for ECR on In–NSC with applied potentials from 0 to −0.8 V (vs. RHE).

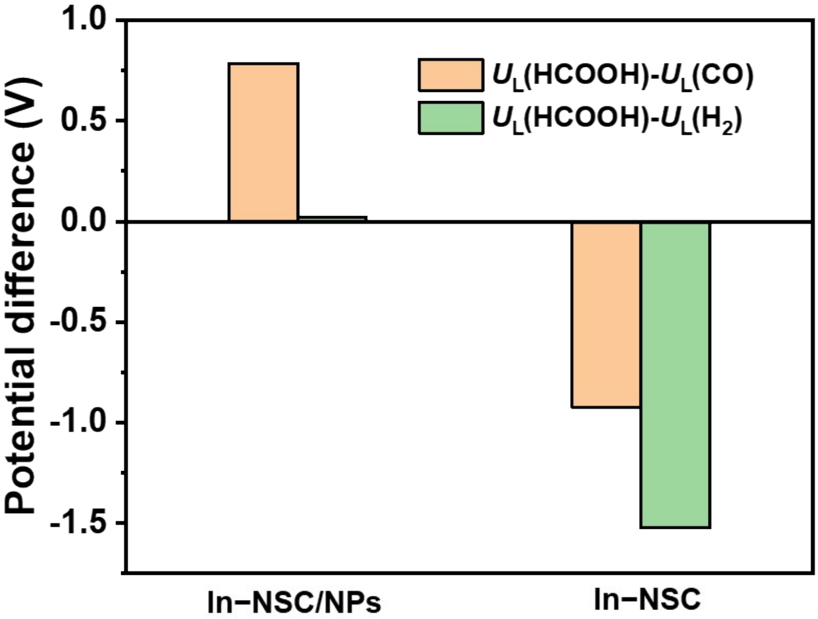

Figure S24. The limiting potential differences of In–NSC/NPs and In–NSC for ECR to HCOOH, CO, and HER.

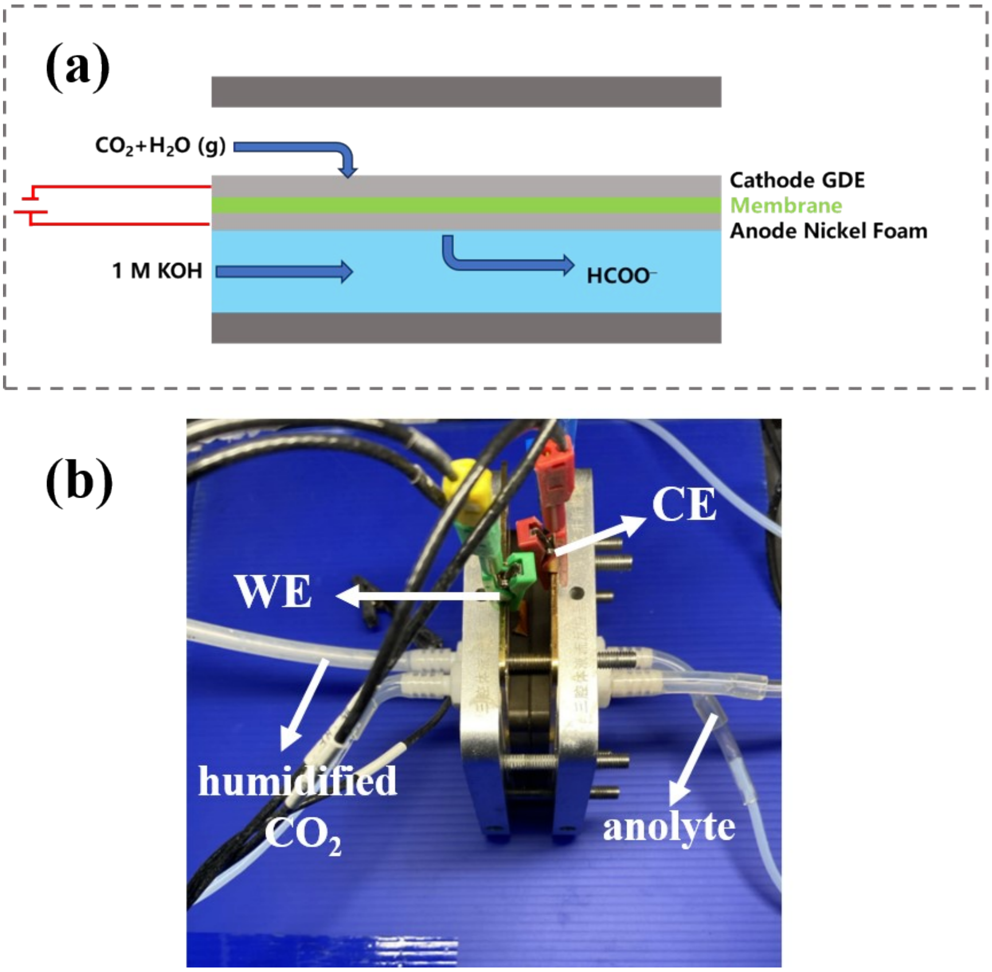

Figure S25. (a) Schematic diagram and (b) photo of an MEA reactor.

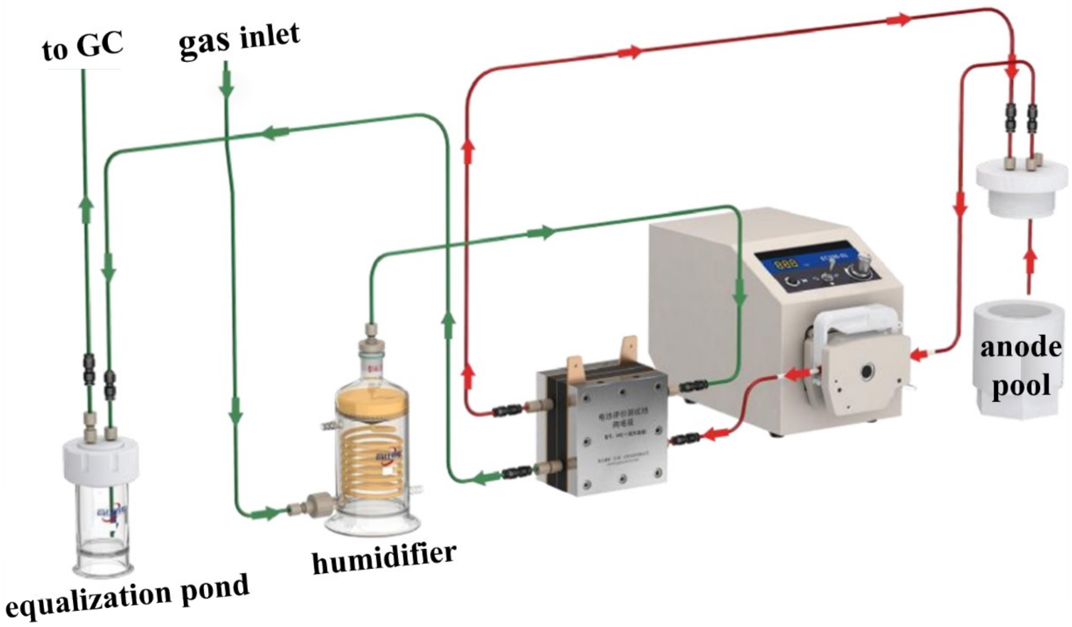

Figure S26. Schematic diagram of an MEA electrolytic system.

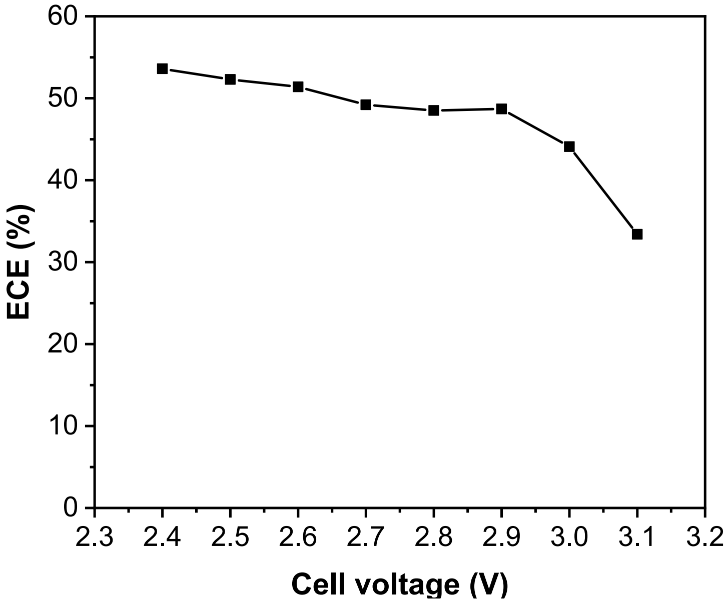

Figure S27. ECE as a function of applied potential on In−NSC/NPs.

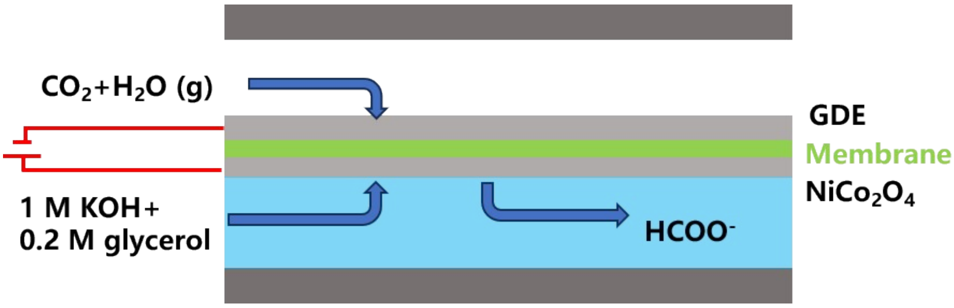

Figure S28. Structural diagram of the ECR//GOR system in an MEA reactor.

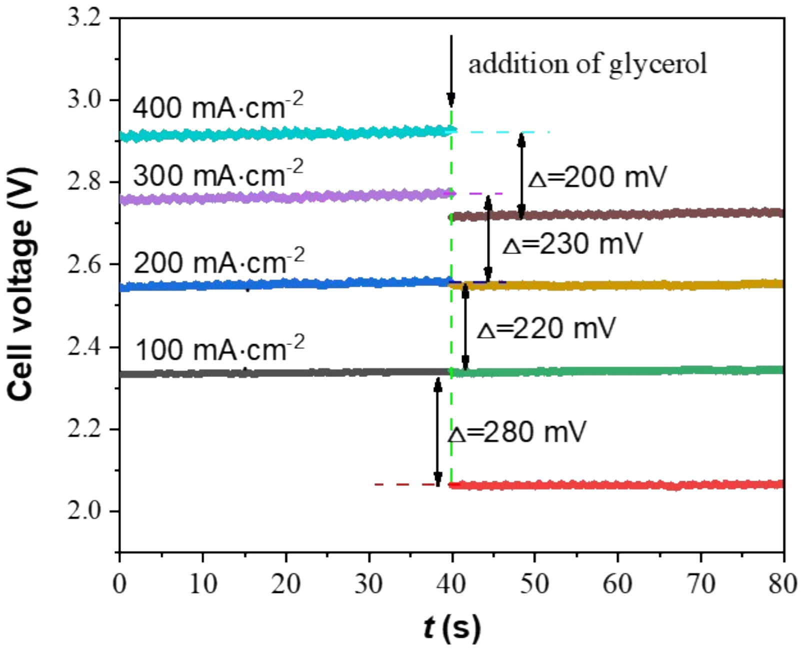

Figure S29. Cell voltage changes of In−NSC/NPs and $NiCo_2O_4$ electrocatalysts in 1 M KOH after injecting 0.2 M glycerol.

Table S1. The contents of In, N, and S in In−NSC/NPs before (named as In−NSC/NPs) and after CO_2 electrolysis (named as In−NSC/NPs-used).

Sample	In content [a] (wt.%)	N content [b] (at. %)	S content [b] (at.%)
In−NSC/NPs	2.91	1.80	0.57
In−NSC/NPs-used	2.89	1.84	0.53

[a] The In content determined by ICP-OES.

[b] The N and S contents determined by XPS.

Table S2. Performance comparison of In−NSC/NPs obtained here with the recently reported typical electrocatalysts for ECR to formate in flow cells.

Catalyst	Electrolyte	$FE_{formate}$ (%)	J (mA·cm^{-2})	Ref.
Ag−In−S	1 M KOH	94	560	7
Bi/Ni−BOC	1 M KOH	90	310	8
Bi−N_2O_2	1 M KOH	90	830	9
Bi_2S_3-derived	1 M KOH	93	2000	10

nBuLi-Bi	1 M $KHCO_3$	92	500	[11]
L-histidine-Bi	1 M KOH	95	350	[12]
Bi[2-MeIm]	1 M KOH	90	1000	[13]
Pb_1Cu	0.5 M $KHCO_3$	96	830	[14]
CuS 811	1 M KOH	85	300	[15]
In/Bi-750	1 M KOH	90	200	[16]
$Bi_{60}In_2NT$	1 M KOH	95	1080	[17]
InP CQDs	1 M KOH	93	930	[18]
s-SnLi	1 M KOH	92	1000	[19]
SAA-ZnBi	1 M KOH	90	1300	[20]
$ZnIn_2S_4$	1 M KOH	99	300	[21]
SnPc-8F@CNTs	1 M KOH	91	450	[22]
In−NSC/NPs	1 M KOH	99	600	This work
In−NSC/NPs	1 M KOH	91	1200	This work

Table S3. Comparison of ECR performance of different electrocatalysts in MEA.

Catalyst	Electrolyte	Electrode area (cm^2)	Voltage (V)	J (mA·cm^{-2})	$FE_{formate}$ (%)	Ref.
In−NSC/NPs	1 M KOH	4	2.9	570	98	This work
Bi-DC	0.1 M $KHCO_3$	4	4.5	200	80	[23]
BiS-1	0.5 M KOH	1	3.86	700	90	[24]
MIL-68(In)-NH_2	1.0 M KOH	4	2.7	258	92	[25]
Bi_2O_3	1.0 M KOH	25	2.27	500	71	[26]
2D-Bi	0.5 M	1	3.21	31	90	[27]

	H_2SO_4					
Bi_2S_3-derived	0.5 M H_2SO_4	4	4.2	295	93	[28]
Pb_1Cu	0.5 M H_2SO_4	3	3.86	133	94	[14]

References

1. G. Wu, X. Dong, J. Mao, G. Li, C. Zhu, S. Li, A. Chen, G. Feng, Y. Song, W. Chen and W. Wei, *Chem. Eng. J.*, 2023, **468**, 143640.

2. G. Kresse and J. Furthmüller, *Phys. Rev. B*, 1996, **54**, 11169−11186.

3. J. P. Perdew, K. Burke and M. Ernzerhof, *Phys. Rev. Lett.*, 1996, **77**, 3865−3868.

4. E. Torres, T. P. Kaloni, Comp. *Mater. Sci.*, 2020, **171**, 109237.

5. S. Grimme, J. Antony, S. Ehrlich and H. Krieg, *J. Chem. Phys.*, 2010, **132**, 154104.

6. V. Wang, N. Xu, J.-C. Liu, G. Tang and W.-T. Geng, *Comput. Phys. Commun.*, 2021, **267**, 108033.

7. J. Zhang, T. Fan, P. Huang, X. Lian, Y. Guo, Z. Chen and X. Yi, *Adv. Funct.* Mater., 2022, **32**, 2113075.

8. C. Ning, Z. Wu, S. Bai, J. Ren, S. Li, W. Xiong, L. Zheng, J. Zheng, Y.F. Song and Y. Zhao, *AIChE J.,* 2023, **70**, e18350.

9. C. Wang, Z. Lv, Y. Liu, R. Liu, C. Sun, J. Wang, L. Li, X. Liu, X. Feng, W. Yang and B. Wang, *Angew. Chem. Int. Ed.,* 2024, **63**, e202404015.

10. L. Lin, X. He, X.G. Zhang, W. Ma, B. Zhang, D. Wei, S. Xie, Q. Zhang, X. Yi and Y. Wang, *Angew. Chem. Int. Ed.,* 2022, **62**, e202214959.

11. L. Fan, C. Xia, P. Zhu, Y. Lu and H. Wang, *Nat. Commun.,* 2020, **11**, 3633.

12. Y. Li, E.P. Delmo, G. Hou, X. Cui, M. Zhao, Z. Tian, Y. Zhang and M. Shao, *Angew. Chem. Int. Ed.,* 2022, **62**, e202313522.

13. M.A.A. Mahbub, J.R.C. Junqueira, X. Wang, J. Zhang, S. Dieckhöfer, S. Seisel, D. Das, W. Schuhmann, *Adv. Funct. Mater.,* 2023, **34**, 2307752.

14. T. Zheng, C. Liu, C. Guo, M. Zhang, X. Li, Q. Jiang, W. Xue, H. Li, A. Li, C.-W. Pao, J. Xiao, C. Xia and J. Zeng, *Nat. Nanotechnol.,* 2021, **16**, 1386–1393.

15. Y. Wang, H. Xu, Y. Liu, J. Jang, X. Qiu, E.P. Delmo, Q. Zhao, P. Gao and M. Shao, *Angew. Chem. Int. Ed.,* 2024, **63**, e202313858.

16. Q. Wang, X. Yang, H. Zang, C. Liu, J. Wang, N. Yu, L. Kuai, Q. Qin, B. Geng, *Small,* 2023, **19**, 2303172.

17. Z. Chen, D. Zhang, Q. Li, H. Zhang, Y. Zhao, Q. Ke, Y. Yan, L. Liu, M. Liu, X. He, *Appl. Catal. B−Environ.,* 2024, **341**, 123342.

18. I. Grigioni, L.K. Sagar, Y.C. Li, G. Lee, Y. Yan, K. Bertens, R.K. Miao, X. Wang, J. Abed, D.H. Won, F.P. García de Arquer, A.H. Ip, D. Sinton and E.H. Sargent, *ACS Energy Lett.,* 2020, **6**, 79−84.

19. S. Yan, C. Peng, C. Yang, Y. Chen, J. Zhang, A. Guan, X. Lv, H. Wang, Z. Wang, T.K. Sham, Q. Han, G. Zheng, *Angew. Chem. Int. Ed.,* 2021*,* **60**, 25945–25949.

20. H. Shen, T. Wang, H. Jiang, P. Zhao, Z. Chen, Y. Feng, Y. Cao, Y. Guo, Q. Zhang, H. Zhang, *Appl Catal B–Environ.,* 2023*,* **339**, 123140.

21. L.-P. Chi, Z.-Z. Niu, X.-L. Zhang, P.-P. Yang, J. Liao, F.-Y. Gao, Z.-Z. Wu, K.-B. Tang, M.-R. Gao, *Nat. Commun.,* 2021, **12**, 5835.

22. B. Chen, H. Zou, L. Gong, H. Zhang, N. Li, H. Pan, K. Wang, T. Yang, Y. Liu, L. Duan, J. Liu, J. Jiang, *Appl Catal B–Environ.,* 2024, **344**, 123650.

23. W. Li, C. Yu, X. Tan, Y. Ren, Y. Zhang, S. Cui, Y. Yang and J. Qiu, *ACS Catal.,* 2024*,* **14**, 8050–8061.

24. Z. Jiang, S. Ren, X. Cao, Q. Fan, R. Yu, J. Yang and J. Mao, *Angew. Chem. Int. Ed.,* 2024, **136**, e202408412.

25. Z. Wang, Y. Zhou, C. Xia, W. Guo, B. You, and B. Xia, *Angew. Chem. Int. Ed.,* 2021, **60**, 19107–19112.

26. L. Hu, J.A. Wrubel, C. M. Baez-Cotto, F. Intia, J. H. Park, A. J. Kropf, N. Kariuki, Z. Huang, A. Farghaly, L. Amichi, P. Saha, L. Tao, D. A. Cullen, D. J. Myers, M. S. Ferrandon and K. C. Neyerlin, *Nat. Commun.,* 2023, **14**, 7605.

27. C. Xia, P. Zhu, Q. Jiang, Y. Pan, W. Liang, E. Stavitski, H. N. Alshareef, H. Wang, *Nat. Energy,* 2019, **4**, 776–785.

28. L. Lin, X. He, X. Zhang, W. Ma, B. Zhang, D. Wei, S. Xie, Q. Zhang, X. Yi and Y. Wang, *Angew. Chem. Int. Ed.,* 2022, **62**, e202214959.